



# New NiMoO<sub>4</sub>/CoMoO<sub>4</sub> composite electrodes for enhanced performance supercapacitors

Yong Zhang<sup>1</sup> · Han-xin Mei<sup>1</sup> · Jing Yang<sup>1</sup> · Shi-wen Wang<sup>1</sup> · Hai-li Gao<sup>1</sup> · Xiao-dong Jia<sup>1</sup> · Ji Yan<sup>1</sup> · Yang Cao<sup>1</sup> · He-wei Luo<sup>1</sup> · Ke-zheng Gao<sup>1</sup>

Received: 6 January 2020 / Revised: 15 January 2020 / Accepted: 19 January 2020 / Published online: 29 January 2020  
© Springer-Verlag GmbH Germany, part of Springer Nature 2020

## Abstract

New NiMoO<sub>4</sub>/CoMoO<sub>4</sub> composite materials on Ni foam were successfully synthesized by a facile hydrothermal method using the mixture powers of Ni(NO<sub>3</sub>)<sub>2</sub>·6H<sub>2</sub>O and Co(NO<sub>3</sub>)<sub>2</sub>·6H<sub>2</sub>O as raw materials. The phase composition, microstructure, and morphology of the as-prepared composites were investigated by XRD, FTIR, SEM, EDS, and XPS. The electrochemical behaviors of the composites were tested by cyclic voltammetry, galvanostatic charge-discharge, and electrochemical impedance spectroscopy. The results indicated that the as-prepared composites are uniformly distributed on the surface of Ni foam with diameters between 2 and 3 μm, and the NiMoO<sub>4</sub>/CoMoO<sub>4</sub> composite displays the best electrochemical properties when the molar ratio of Ni/Co is 1:1. In 3 mol L<sup>-1</sup> KOH electrolytes with current densities of 1, 4, 7, and 10 A g<sup>-1</sup>, the discharge specific capacitance of NiMoO<sub>4</sub>/CoMoO<sub>4</sub> composite is 2221, 1868, 1678, and 1568 F g<sup>-1</sup>, respectively, indicating its promising applications for high electrochemical performance energy storage device.

**Keywords** Hydrothermal method · NiMoO<sub>4</sub>/CoMoO<sub>4</sub> composites · Ni foam · Specific capacitance · Electrochemical performance

## Introduction

Energy is the material basis of human activities, the core driving force for economic development, and the essential condition for a country's core competitiveness and sustainable economic and social development [1–7]. Supercapacitors (SCs), also known as electrochemical capacitors, electrochemical double-layer capacitors, pseudocapacitors, ultracapacitors, power capacitors, and gold capacitors, etc. [8, 9], are devices that store energy through a double electrical layer at the electrode/electrolyte interface, or through the electrochemical Faraday redox reactions [10, 11]. As a new type of energy storage device with high efficiency and cleanness, SC has higher energy density and power density than traditional

dielectric capacitor. Compared with traditional battery, supercapacitor has the advantages of high power density, fast charging and discharging speed, long cycle life, and wide working temperature range [12]. It can be widely used in backup batteries, energy storage, and auxiliary peak power and so on. The situation has great market value and commercial potential in industrial control, military, electric power, new energy vehicles, etc. [13, 14]. However, the low energy density of SCs is an important reason to limit their development. At present, the main solution is to develop electrode materials with high electrochemical performance. Previous studies on electrode materials for SCs are mainly focused on transition metal oxides or hydroxides with pseudocapacitive properties, for example, NiO [15, 16], RuO<sub>2</sub> [17], MnO<sub>2</sub> [18], Co(OH)<sub>2</sub> [19], V<sub>2</sub>O<sub>5</sub> [20], and Ni(OH)<sub>2</sub> [21]. The RuO<sub>2</sub> exhibits the best electrochemical performance. However, its high price and toxicity limit its wide commercial application [22].

In recent years, the multi-hybrid nanomaterials of SCs (such as NiMoO<sub>4</sub> [23–25], CoMoO<sub>4</sub> [26], ZnCo<sub>2</sub>O<sub>4</sub> [27], NiCo<sub>2</sub>O<sub>4</sub> [28], MnMoO<sub>4</sub> [29], NiO@CeO<sub>2</sub> [30], NiO@MnO<sub>2</sub> [31], NiCo<sub>2</sub>O<sub>4</sub>@NiWO<sub>4</sub> [32], NiMoO<sub>4</sub>/CoMoO<sub>4</sub> [33], NiCo<sub>2</sub>S<sub>4</sub>@NiMoO<sub>4</sub> [34], and CoMoO<sub>4</sub>-NiMoO<sub>4</sub>·xH<sub>2</sub>O [35]) have become a strong exploration trend due to their intrinsic properties, such as low cost, natural abundance, reliable redox

✉ Yong Zhang  
zy@zzuli.edu.cn

Hai-li Gao  
gaohaili@zzuli.edu.cn

<sup>1</sup> Department of Material and Chemical Engineering, Zhengzhou University of Light Industry, Zhengzhou 450001, People's Republic of China

transformation, and synergistic effects [36]. It is worth mentioning that the good electrochemical activity of nickel ions and the better conductivity of molybdenum elements can be attributed to the excellent electrochemical capacitance of the obtained bimolybdate [37, 38]. For examples, Huang et al. [39] successfully prepared wall-like hierarchical metal oxide  $\text{MMoO}_4$  ( $M = \text{Ni}, \text{Co}$ ) nanosheet arrays electrode material by a facile hydrothermal method, which exhibited a high specific capacitance of 1483 and  $452 \text{ F g}^{-1}$  for  $\text{NiMoO}_4$  and  $\text{CoMoO}_4$  at a current density of  $2 \text{ A g}^{-1}$ . Cai et al. [40] synthesized  $\text{NiMoO}_4$  nanospheres and nanorods by a facile hydrothermal method, which exhibited a high specific capacitance of  $974.4 \text{ F g}^{-1}$  at a current density of  $1 \text{ A g}^{-1}$ . Furthermore, Tian et al. [41] rationally designed porous worm-like  $\text{NiMoO}_4$  by electrostatic spinning, which offered good rate capability ( $860.3 \text{ F g}^{-1}$  at a current density of  $20 \text{ A g}^{-1}$ ), high specific capacitance ( $1088.5 \text{ F g}^{-1}$  at a current density of  $1 \text{ A g}^{-1}$ ), and long cycle life with a capacity retention of 73.9% after 5000 cycles. Usually,  $\text{NiMoO}_4$  electrode material can offer high capacitance and low cycle stability, while  $\text{CoMoO}_4$  exhibits a lower capacitance and good rate capability [33]. Zhao et al. [42] prepared  $\text{CoMoO}_4$  nanorod electrode, which exhibited a specific capacitance of  $89.5 \text{ F g}^{-1}$  at a current density of  $1 \text{ mA cm}^{-2}$ . Veerasubramani et al. [43] synthesized plate-like  $\text{CoMoO}_4$  nanostructures via a facile sonochemical approach, which showed a specific capacitance of  $133 \text{ F g}^{-1}$  at a current density of  $1 \text{ mA cm}^{-2}$ , and the capacitance retention is about 84% after 1000 cycles. Zhang et al. [44] prepared  $\text{NiMoO}_4/\text{CoMoO}_4$  nanospheres on Ni foam, which delivered a greatly enhanced specific capacitance of  $1601.6 \text{ F g}^{-1}$  at a current density of  $2 \text{ A g}^{-1}$ , as well as better cycling stability and rate capability than pure  $\text{NiMoO}_4$  or  $\text{CoMoO}_4$  material. Therefore, a large number of scientists trend to investigate composite electrode materials for SCs, and use the synergistic effect between different components to increase the rapid diffusion and transport of electrons and ions, which illustrate that the electrochemical performance of the composite material is superior to that of the single material.

However, most current  $\text{NiMoO}_4$  or  $\text{CoMoO}_4$  literatures [33, 45–47] adopt cladding paste electrode, making its actual discharge capacity much smaller than its theoretical value. Based on the above considerations, an integrated  $\text{NiMoO}_4/\text{CoMoO}_4$  electrode (with binder-free) based on Ni foamed is prepared by a simple hydrothermal method, which is helpful to reduce the contact resistance between electrode materials and collector, and to improve the capacitive performance. As far as we know, the novel  $\text{NiMoO}_4/\text{CoMoO}_4$  micron structure has rarely been reported. And the excellent electrochemical properties of the composites are attributed to the synergistic effect of  $\text{NiMoO}_4$  and  $\text{CoMoO}_4$ . What's more, the unique structure can provide channels for rapid diffusion process and enrich active reaction sites; shorten electron/ion transport pathways, improving the redox reaction of active material not

only on the surface of electrode but also in the electrolyte; and then improve the utilization of active materials. Using these advantages, the as-prepared  $\text{NiMoO}_4/\text{CoMoO}_4$  electrode materials have great potential application value in the development of electrochemical energy storage devices.

## Experimental

### Material preparation

Nickel foam was cleaned with acetone, deionized water, hydrochloric acid, and deionized water for 10 min through ultrasonic cleaning, and then completely dried in air. In the typical hydrothermal synthesis process, all reagents are used as raw materials without further purification. The molar ratios of Ni and Co were controlled to be 1:2, 1:1, 2:1, 3:1, 4:1, and 5:1, respectively. The mass of  $\text{Ni}(\text{NO}_3)_2 \cdot 6\text{H}_2\text{O}$  and  $\text{Co}(\text{NO}_3)_2 \cdot 6\text{H}_2\text{O}$  at different nickel-cobalt ratios is calculated, and then, 0.4839 g  $\text{Na}_2\text{MoO}_4 \cdot 2\text{H}_2\text{O}$  and 0.1089 g Na acetate are weighed. The volume ratio of water to ethanol is 2:1, that is, 40 mL water and 20 mL ethanol are mixed evenly and divided into 3 equal parts to dissolve the above substances. Then, the  $\text{Ni}(\text{NO}_3)_2$  solution,  $\text{Co}(\text{NO}_3)_2$  solution, and Na acetate solution were added to  $\text{Na}_2\text{MoO}_4$  solution drop by drop and stirred fully under a magnetic stirrer. After that, the homogeneous solution and the prepared nickel foam are transferred to the Teflon-lined stainless steel autoclave. The hydrothermal reaction was maintained at  $150 \text{ }^\circ\text{C}$  for 6 h. After a reactor was naturally cooled to room temperature, a precursor was washed several times with distilled water and anhydrous ethanol, and then dried completely in air at  $60 \text{ }^\circ\text{C}$  throughout the night. Finally, the  $\text{NiMoO}_4/\text{CoMoO}_4$  composite material was obtained after annealing at  $300 \text{ }^\circ\text{C}$  for 5 h.

### Structure characterizations

The phase and crystal structure of the prepared samples were examined by X-ray powder diffraction (XRD, D8, Bruker) equipped with Cu  $K\alpha$  radiation in the  $2\theta$  range of  $10\text{--}80^\circ$  at a scanning rate of  $4^\circ \text{ min}^{-1}$ . The chemical composition of the samples were determined by Fourier transform infrared spectroscopy (FTIR). The morphology and microstructures of the as-products were characterized by scanning electron microscopy (SEM; JSM 6490) and energy-dispersive spectrometry (EDS). The surface chemical compositions of the obtained sample were analyzed by X-ray photoelectron spectroscopy (XPS, ESCALAB 250Xi) with an Al  $K\alpha$  source.

### Electrochemical measurements

The electrochemical performance of the  $\text{NiMoO}_4/\text{CoMoO}_4$  composites was examined by CHI 660E electrochemical

workstation using three-electrode cell system in 3 mol L<sup>-1</sup> KOH aqueous solution. The prepared NiMoO<sub>4</sub>/CoMoO<sub>4</sub>, platinum foil, and Hg/HgO were used as a working electrode, counter electrode, and reference electrode, respectively. The electrochemical impedance spectroscopy (EIS) measurement is also operated in the frequency range of 0.01–100 kHz with AC amplitude of 5 mV. The specific capacitance ( $C_m$ , F g<sup>-1</sup>), energy density ( $E$ , Wh kg<sup>-1</sup>), and power density ( $P$ , W kg<sup>-1</sup>) were calculated using the following equations [48]:

$$C_m = C/m = \frac{i \times \Delta t}{m \times \Delta u} \quad (1)$$

where  $i$  (A),  $m$  (g),  $\Delta t$  (s), and  $\Delta u$  (V) represent the discharge current, the mass of active electrode material, the total discharge time, and the potential window, respectively.

## Results and discussion

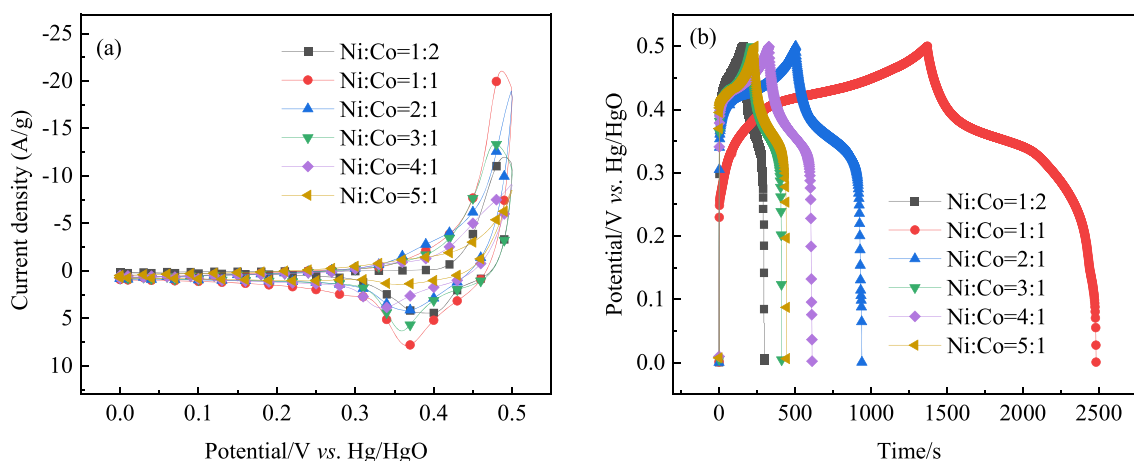
### Determination of the optimum ratio sample

Figure 1a displays the typical cyclic voltammetry (CV) curves of NiMoO<sub>4</sub>/CoMoO<sub>4</sub> composite electrodes with different Ni/Co molar ratios at a scan rate of 5 mV s<sup>-1</sup> recorded in a potential window of 0–0.5 V. Apparently, the CV curves of the resulting NiMoO<sub>4</sub>/CoMoO<sub>4</sub> composite electrode supply typical Faradaic capacitive behavior with a pair of well-defined redox peaks are based on Ni and Co diffusion controlled reversibly changing their oxidation states (Ni<sup>2+</sup>/Ni<sup>3+</sup> and Co<sup>2+</sup>/Co<sup>3+</sup>) [49], which is distinct from that of EDLCs characterized by nearly a rectangular shape. And the oxidation peak potential and reduction peak potential of NiMoO<sub>4</sub>/CoMoO<sub>4</sub> composites are about 0.47 V and 0.37 V, respectively. Furthermore, although Mo is a transition metal, it does not

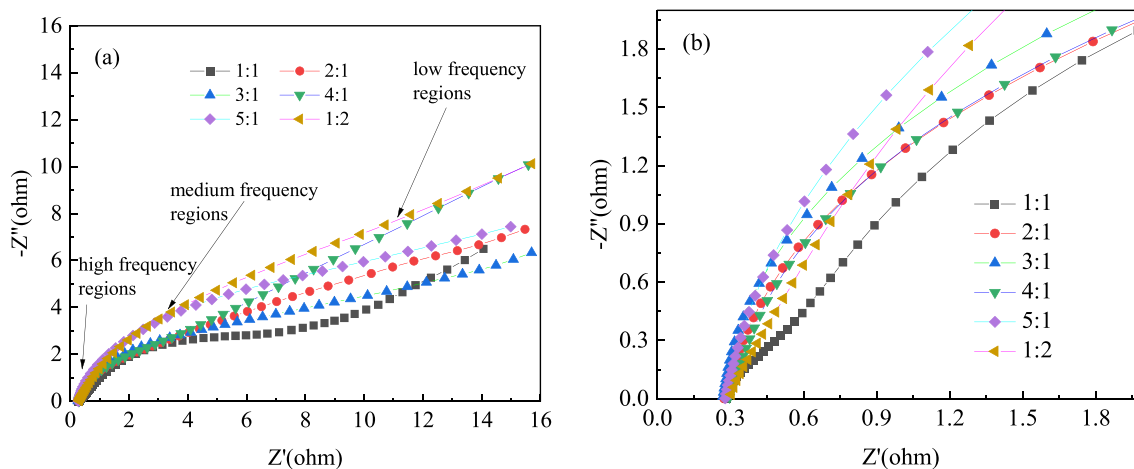
participate in the redox reaction directly, but rather enhances the electrical conductivity, thus improving the electrochemical performance of the electrode [50].

In order to further compare and analyze the electrochemical properties of NiMoO<sub>4</sub>/CoMoO<sub>4</sub> composite electrodes, a series of experiments on Ni/Co molar ratio were carried out, and the corresponding galvanostatic charge-discharge (GCD) curves recorded in a potential window of 0–0.5 V at 1 A g<sup>-1</sup> are shown in Fig. 1b. The GCD curves of NiMoO<sub>4</sub>/CoMoO<sub>4</sub> composite electrodes displayed lines with charge-discharge platform rather than smooth lines, which indicates the pseudocapacitive nature and consistent with the CV results. The near symmetry of the GCD curves indicates that the Faraday redox reaction is highly reversible. More importantly, according to Eq. (1), the specific capacitance of the electrode can be calculated using the charge-discharge curve. A maximum specific capacitance was observed for the composite with a Ni/Co mass ratio of 1:1, which may be promising candidates for the practical application of SCs.

The electrochemical impedance spectroscopy (EIS) is used to investigate the internal resistance of the electrode material, and the resistance between the electrode material and the electrolyte. Figure 2 shows the EIS plots of NiMoO<sub>4</sub>/CoMoO<sub>4</sub> composites with different Ni/Co molar ratios recorded from 0.01–100 kHz with a perturbation amplitude of 5 mV. Figure 2a shows a semicircle section in the high-frequency region and a slant line in the low-frequency region. All the plots are almost the same, including semicircles and oblique lines. High-frequency semicircles represent the induced resistance caused by electron transfer of interfacial active substances. Diameter determines the resistance of electron transfer on the surface of electrodes, and the sloped lines at the low frequency region represent the Warburg impedance caused by diffusion [51]. In addition, the intercepts of the semicircles and the real axis at high frequency can also be obtained.



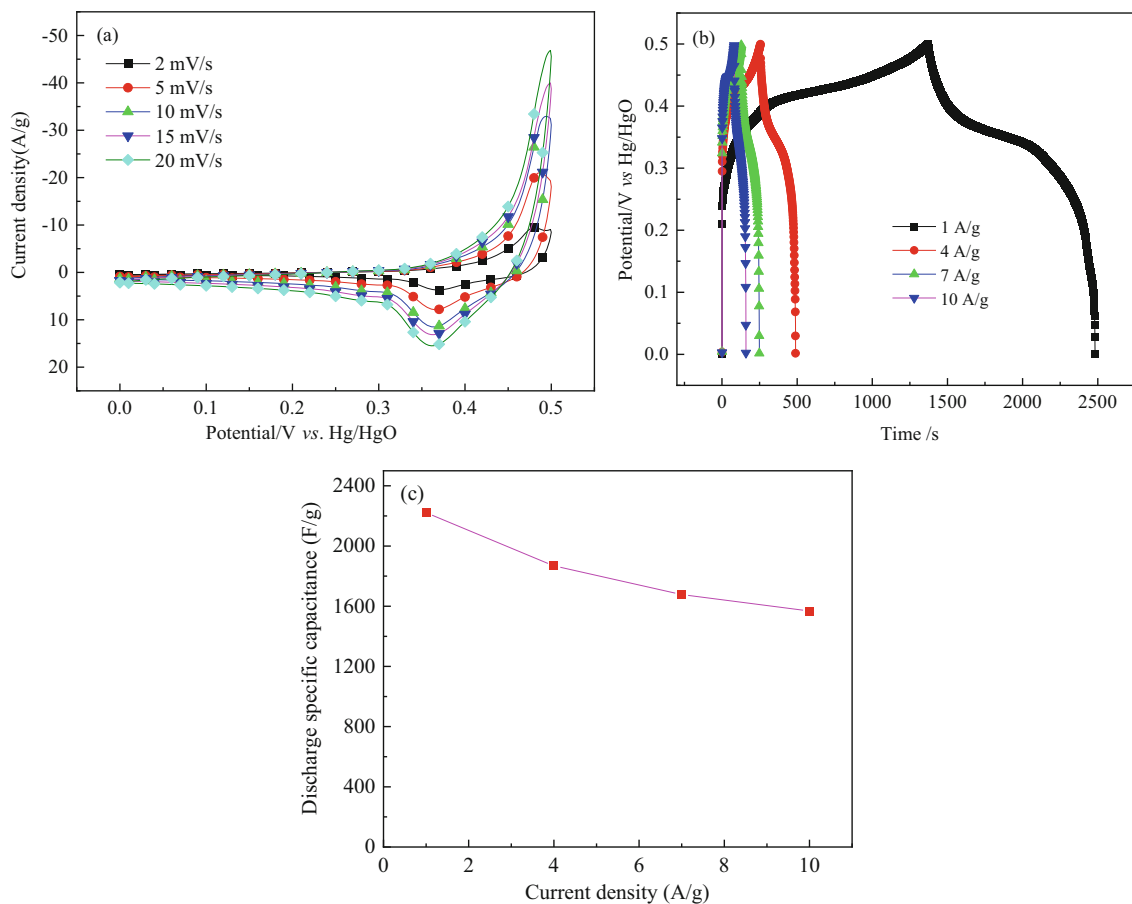
**Fig. 1** **a** CV curves of NiMoO<sub>4</sub>/CoMoO<sub>4</sub> composite electrodes with different Ni/Co molar ratios (1:2, 1:1, 2:1, 3:1, 4:1, and 5:1) at 5 mV s<sup>-1</sup>. **b** GCD curves of NiMoO<sub>4</sub>/CoMoO<sub>4</sub> composite electrodes with different Ni/Co molar ratios (1:2, 1:1, 2:1, 3:1, 4:1, and 5:1) at 1 A g<sup>-1</sup>



**Fig. 2** **a** EIS plots of NiMoO<sub>4</sub>/CoMoO<sub>4</sub> composite electrodes with different Ni/Co molar ratios (1:2, 1:1, 2:1, 3:1, 4:1, and 5:1). **b** The enlarged EIS at the high-frequency region

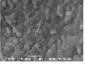
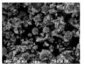
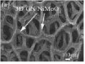
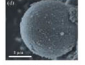
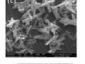
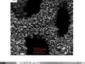
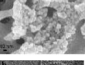

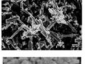
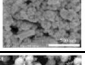
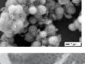
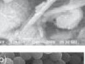
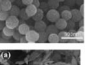
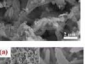

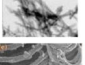
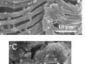
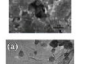
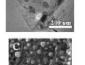
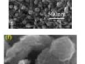


Figure 2b shows the intercepts of NiMoO<sub>4</sub>/CoMoO<sub>4</sub> composites with different Ni/Co molar ratios are approximately the same. In other words, the equivalent series resistance does not change much. The slope value of the composites with a Ni/Co molar ratio of 1:1 is higher than that of other samples, which

indicates that the Warburg impedance is smaller and the diffusion impedance of the active substance in the electrolyte is smaller, which thus accelerates the diffusion of ions in active substances and electrolytes, as well as the transfer of electrons and ions, and improves the degree of the Faraday reaction



**Fig. 3** **a** CV curves of NiMoO<sub>4</sub>/CoMoO<sub>4</sub> composite electrode with Ni/Co molar ratio 1:1 at various scan rates of 2, 5, 10, 15, and 20 mV s<sup>-1</sup>. **b** GCD curves of NiMoO<sub>4</sub>/CoMoO<sub>4</sub> composite electrode with Ni/Co molar ratio 1:1 at various current densities of 1, 4, 7, and 10 A g<sup>-1</sup>. **c** Specific capacitances of the electrode as a function of current densities

**Table 1** Comparison with previously reported supercapacitor electrode materials

Electrode materials	Morphology	Specific capacitance (F	Specific capacitance (F	Reference
		g <sup>-1</sup> ) (low current density)	g <sup>-1</sup> ) (high current density)	
NiMoO <sub>4</sub> /CoMoO <sub>4</sub> (this work)		2221 (1 A g <sup>-1</sup> )	1568 (10 A g <sup>-1</sup> )	
MnO <sub>2</sub>		258.7 (0.1 A g <sup>-1</sup> )	165.3 (0.3 A g <sup>-1</sup> )	[57]
NG/NiMoO <sub>4</sub>		1913 (1 A g <sup>-1</sup> )	1350 (10 A g <sup>-1</sup> )	[58]
Ni <sub>1.4</sub> Co <sub>0.6</sub> P@C		1571.3 (1 A g <sup>-1</sup> )	1480 (10 A g <sup>-1</sup> )	[59]
NiCo <sub>2</sub> S <sub>4</sub>		1130 (0.4 A g <sup>-1</sup> )	960 (5 A g <sup>-1</sup> )	[60]
Co <sub>3</sub> O <sub>4</sub>		1060.0 (1 A g <sup>-1</sup> )	642.5 (10 A g <sup>-1</sup> )	[61]
ZnCo <sub>2</sub> O <sub>4</sub>		843 (1 A g <sup>-1</sup> )	613 (3 A g <sup>-1</sup> )	[62]
Co <sub>3</sub> O <sub>4</sub> /CdO		453.6 (2 A g <sup>-1</sup> )	366 (10 A g <sup>-1</sup> )	[63]
NiCoFeO <sub>4</sub>		1263 (1 A g <sup>-1</sup> )	458 (11 A g <sup>-1</sup> )	[64]
NaNi <sub>0.33</sub> Co <sub>0.67</sub> PO <sub>4</sub> ·H <sub>2</sub> O		828 (1 A g <sup>-1</sup> )	734 (10 A g <sup>-1</sup> )	[65]
PANI/NiO/SGO		1350 (1 A g <sup>-1</sup> )	775 (10 A g <sup>-1</sup> )	[66]
NiMoO <sub>4</sub> /MWCNTs		805 (1 A g <sup>-1</sup> )	584 (10 A g <sup>-1</sup> )	[67]
NCSs@Fe <sub>3</sub> O <sub>4</sub>		206 (1 A g <sup>-1</sup> )	90 (10 A g <sup>-1</sup> )	[68]
NiCo-MOF@PNTs		1109 (0.5 A g <sup>-1</sup> )	957 (10 A g <sup>-1</sup> )	[69]
NiCo <sub>2</sub> O <sub>4</sub>		790 (1 A g <sup>-1</sup> )	710 (10 A g <sup>-1</sup> )	[70]
Ni <sub>2</sub> P <sub>2</sub> O <sub>7</sub>		772.5 (1 A g <sup>-1</sup> )	544 (8 A g <sup>-1</sup> )	[71]
L-AC@MnO <sub>2</sub>		248 (1 A g <sup>-1</sup> )	184 (10 A g <sup>-1</sup> )	[72]
NiO/Ni <sub>3</sub> S <sub>2</sub> @graphite		768 (1 A g <sup>-1</sup> )	549 (10 A g <sup>-1</sup> )	[73]
Co <sub>9</sub> S <sub>8</sub> /S-doped rGO		708.3 (1 A g <sup>-1</sup> )	590 (10 A g <sup>-1</sup> )	[74]
NiO/NiS@CNT		809.7 (1 A g <sup>-1</sup> )	765.1 (10 A g <sup>-1</sup> )	[75]
Co <sub>3</sub> O <sub>4</sub> -PANI@ZIF-8NPC		1407 (1 A g <sup>-1</sup> )	742 (10 A g <sup>-1</sup> )	[76]
NiMoO <sub>4</sub> /CoMoO <sub>4</sub>		740 (1 A g <sup>-1</sup> )	474 (10 A g <sup>-1</sup> )	[77]

[52]. As mentioned above, when the molar ratio of Ni/Co is 1:1, the obtained NiMoO<sub>4</sub>/CoMoO<sub>4</sub> composite has the best electrochemical performance.

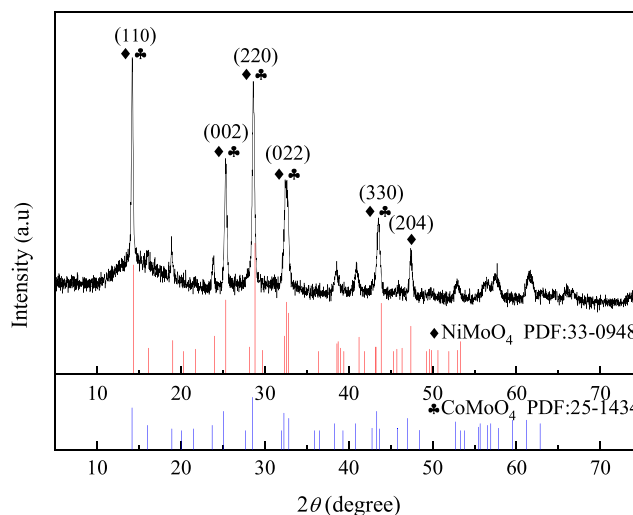
### Characterization of the optimum ratio sample

Figure 3a shows the CV curves of NiMoO<sub>4</sub>/CoMoO<sub>4</sub> composite with Ni/Co molar ratio 1:1 at various scan rates of 2, 5, 10, 15, and 20 mV s<sup>-1</sup> in the potential range of 0–0.5 V. With the increase of scanning rate from 2 to 20 mV s<sup>-1</sup>, the redox peak potential almost remains unchanged, but the area of CV curve and peak current gradually increased. Therefore, accelerating electron transport and optimizing electrode structure can realize the rapid redox reaction process for energy storage. The shape of CV curve changed slightly, which indicated that the sample had good rate characteristics and excellent electrochemical properties [53–56].

Figure 3b shows the GCD curves of NiMoO<sub>4</sub>/CoMoO<sub>4</sub> composite with Ni/Co molar ratio 1:1 at various current densities of 1, 4, 7, and 10 A g<sup>-1</sup>, respectively. A well-defined platform can be observed in the GCD curves, and the discharge specific capacitance calculated according to Eq. (1) is shown in Fig. 3c. When the discharge current densities are 1, 4, 7, and 10 A g<sup>-1</sup>, the excellent discharge specific capacitances of the composite are 2221, 1868, 1678, and 1568 F g<sup>-1</sup>, respectively. When the current density increases from 1 to 10 A g<sup>-1</sup>, the discharge time and discharge specific capacitance decrease gradually. It is impressive that the highest discharge specific capacitance is 2221 F g<sup>-1</sup> at 1 A g<sup>-1</sup>. When the current density increases to 10 A g<sup>-1</sup>, the discharge specific capacitance (1568 F g<sup>-1</sup>) is 70.6% retention for 1 A g<sup>-1</sup>. However, according to literature report [41], the specific capacitance of NiMoO<sub>4</sub> is 1088.5 F g<sup>-1</sup> at current density of 1 A g<sup>-1</sup>, which indicates that the synergistic effect of NiMoO<sub>4</sub>/CoMoO<sub>4</sub> composite makes it a high capacity and excellent rate material [48].

To demonstrate the advantages of the material, in Table 1, we compare the related properties (such as specific capacitance at low and high current densities) of NiMoO<sub>4</sub>/CoMoO<sub>4</sub> electrode with other recently reported transition metal oxide-based electrodes in the literature. Compared with previous studies, the NiMoO<sub>4</sub>/CoMoO<sub>4</sub> electrode reported in this paper has higher specific capacitance and bigger rate capability. This is due to the fact that NiMoO<sub>4</sub> and CoMoO<sub>4</sub> components exhibit good synergies, making the composite exhibit better capacitive properties, indicating that NiMoO<sub>4</sub>/CoMoO<sub>4</sub> composite is an ideal material for building SCs.

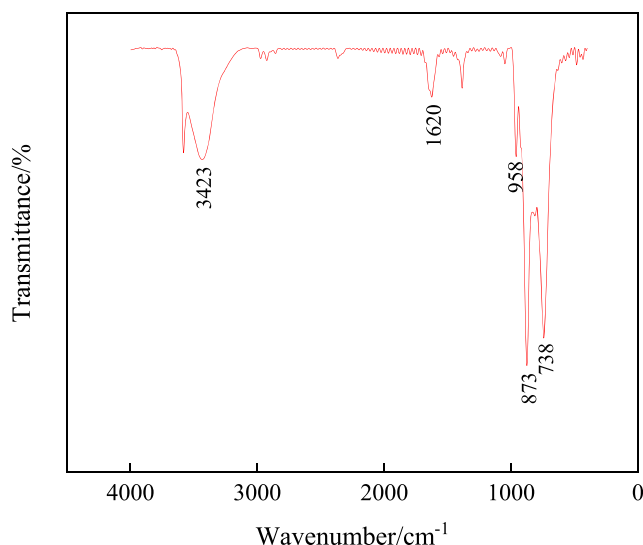
Figure 4 shows the XRD results of the as-synthesized NiMoO<sub>4</sub>/CoMoO<sub>4</sub> composite with Ni/Co molar ratio 1:1. The diffraction patterns of single NiMoO<sub>4</sub> and pure CoMoO<sub>4</sub> are consistent with the standard spectra of NiMoO<sub>4</sub> (JCPDS card no. 33-0948) and CoMoO<sub>4</sub> (JCPDS



**Fig. 4** XRD pattern of NiMoO<sub>4</sub>/CoMoO<sub>4</sub> composite with Ni/Co molar ratio 1:1

card no. 25-1434), respectively. In addition, the present both the characteristic diffraction peaks of NiMoO<sub>4</sub> and CoMoO<sub>4</sub> phases are appeared in the spectra of NiMoO<sub>4</sub>/CoMoO<sub>4</sub> composite, indicating the coexistence of NiMoO<sub>4</sub> and CoMoO<sub>4</sub>. For the hybrid composite, the diffraction peaks at 14.3°, 25.3°, 28.8°, 32.7°, 43.8°, and 47.5° are attributed to the reflections of (110), (002), (220), (022), (330), and (204) planes, which is in good agreement with the standard spectrum of NiMoO<sub>4</sub> [51]. In addition, the other diffraction peaks occurring at 14.1°, 25.1°, 28.5°, 32.3°, and 43.2° can be readily indexed to CoMoO<sub>4</sub> [78–80]. Therefore, XRD analysis shows that we have successfully synthesized NiMoO<sub>4</sub>/CoMoO<sub>4</sub> composite on Ni foams. Besides, there are still some weak peaks, showing a lower crystallinity.

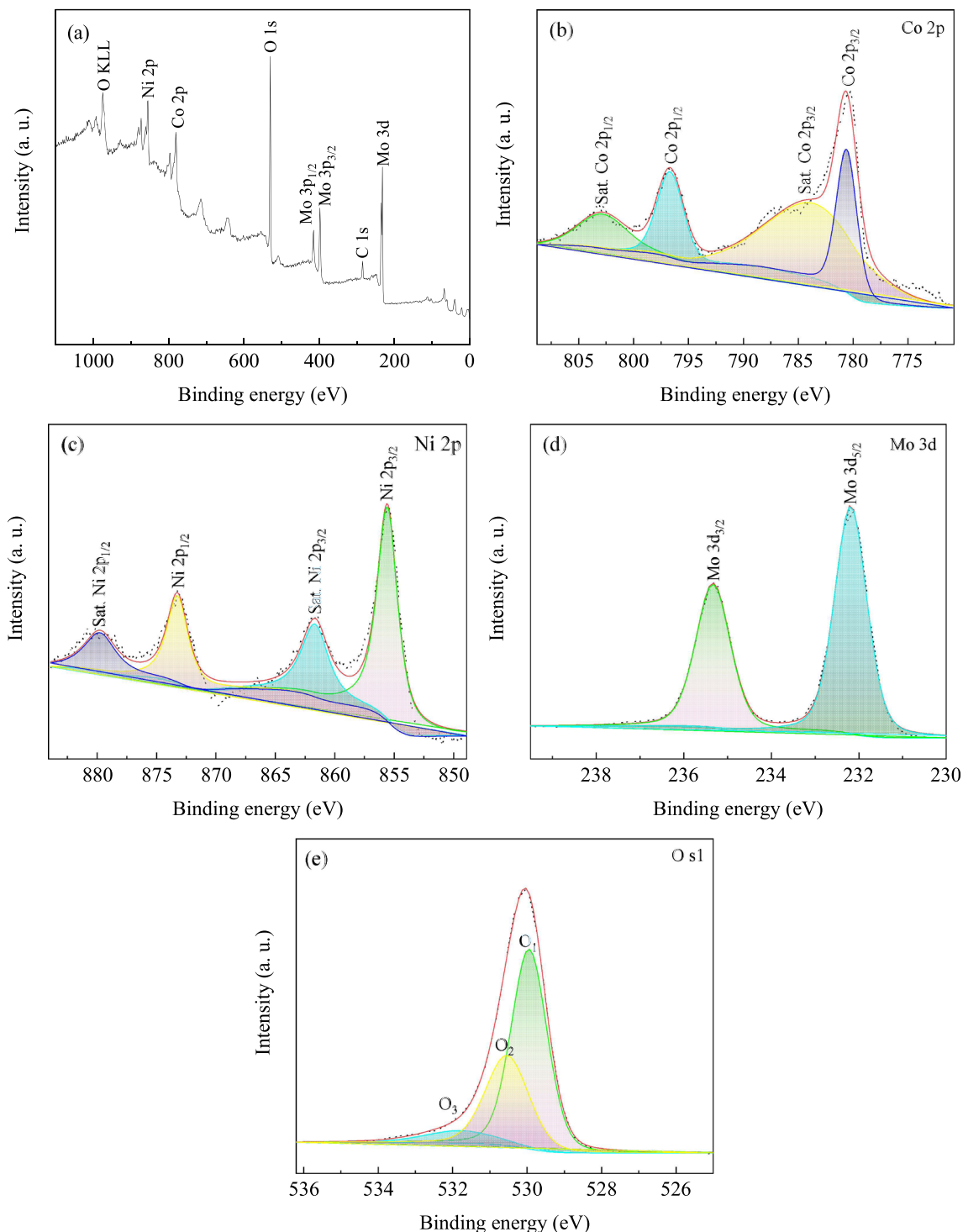
Figure 5 shows the FTIR spectra of the prepared samples. Obviously, the typical peaks 958 cm<sup>-1</sup>, 873 cm<sup>-1</sup>, and



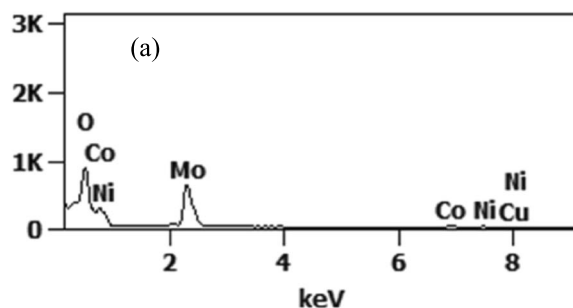
**Fig. 5** FTIR spectra of NiMoO<sub>4</sub>/CoMoO<sub>4</sub> composite with Ni/Co molar ratio 1:1

738  $\text{cm}^{-1}$  were observed on the  $\text{NiMoO}_4/\text{CoMoO}_4$  curve, corresponding to the absorption vibrations of Mo–O, Co–O, and Ni–O bonds, respectively. The extra peak at 3423  $\text{cm}^{-1}$  is due to the stretching vibration of –OH. In addition, the bending vibration of the FTIR peak at 1620  $\text{cm}^{-1}$  is due to the physical adsorption of water molecules in the sample, this can indicate the presence of crystal water in the sample [81].

In order to further investigate the valence states of elements in the as-synthesized  $\text{NiMoO}_4/\text{CoMoO}_4$  composite, XPS experiments were performed, and the corresponding results are shown in Fig. 6. In detail, the survey spectra (Fig. 6a) of the composite sample exhibits the distinct peaks of Co 2p, Ni 2p, Mo 3d, and O 1s peaks located at 781.2, 854.7, 231.2, and 530.1 eV, revealing the presence of Co,



**Fig. 6** a Full XPS spectra and the deconvoluted b Co 2p, c Ni 2p, d Mo 3d, and e O 1s spectra of  $\text{NiMoO}_4/\text{CoMoO}_4$  composite



Element	Net	Weight %	Weight %	Atom %	Atom %
Line	Counts		Error		Error
O K	4500	27.91	± 0.79	65.94	± 1.88
Co L	1259	12.98	± 0.90	8.32	± 0.58
Ni L	1540	9.84	± 0.45	6.33	± 0.29
Cu L	0	0.00	---	0.00	± 0.00
Mo L	10832	49.27	± 0.99	19.41	± 0.39
<b>Total</b>		100.00		100.00	

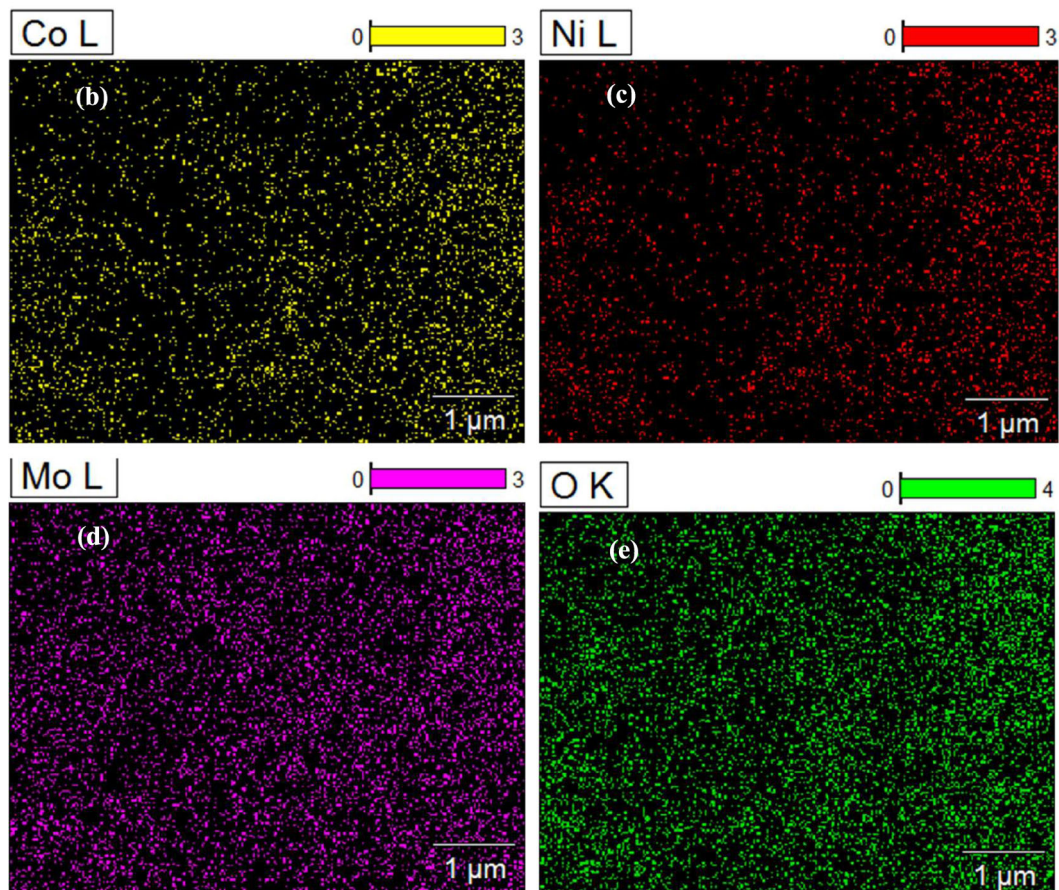
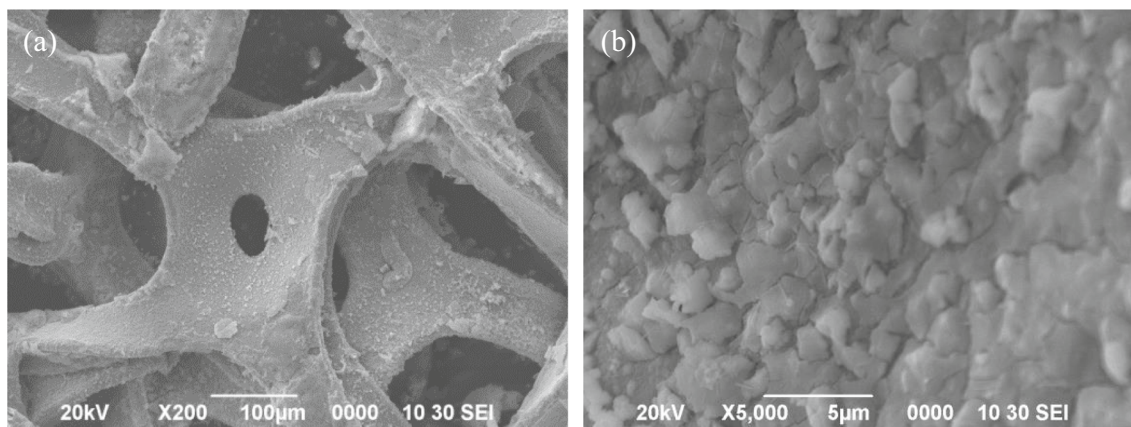


Fig. 7 a EDS pattern of NiMoO<sub>4</sub>/CoMoO<sub>4</sub> composite with Ni/Co molar ratio 1:1. EDS distribution mapping of b Co, c Ni, d Mo, and e O





**Fig. 8** a, b Typical SEM images of NiMoO<sub>4</sub>/CoMoO<sub>4</sub> composite with Ni/Co molar ratio 1:1

Ni, Mo, and O elements, respectively. Figure 6b shows the Co 2p core level spectrum; the two main fitted peaks at 796.7 and 780.6 eV, accompanied two diminutive satellite peaks at 803.1 and 784.2 eV, are assigned to Co 2p<sub>1/2</sub> and Co 2p<sub>3/2</sub> energy level, respectively. The primary peaks and shakeup satellite peaks of Co 2p<sub>1/2</sub> and Co 2p<sub>3/2</sub> indicate the Co<sup>2+</sup> valence state [33]. As depicted in Fig. 6c, the Ni 2p spectrum was fitted by four peaks. The major peak at 873.4 eV and its satellite peak at 879.9 eV are owing to Ni 2p<sub>1/2</sub> level, whereas those at 855.6 and 861.7 eV are ascribed to Ni 2p<sub>3/2</sub> level. Further, the gap in binding energy between the main peaks of Ni 2p<sub>1/2</sub> and Ni 2p<sub>3/2</sub> is 17.8 eV, proving the existence of the Ni<sup>2+</sup> oxidation state [44]. The deconvoluted Mo 3d spectrum (Fig. 6d) exhibits two major peaks at 235.3 and 232.2 eV which can be assigned to Mo 3d<sub>3/2</sub> and 3d<sub>5/2</sub> energy level, respectively. The two peaks are separated by a binding energy of 3.1 eV, confirming the existence of an oxidation state of Mo<sup>6+</sup> [82], which is consistent with the previous reports [83]. In addition, the O 1s spectrum (Fig. 6e) can deconvoluted into three oxygen peaks, located at 529.9, 530.5, and 532.2 eV of O<sub>1</sub>, O<sub>2</sub>, and O<sub>3</sub> components, respectively. The O<sub>1</sub> component is related to metal–oxygen bond, while O<sub>2</sub> component is attributed to functional groups and defect sites, and O<sub>3</sub> component is ascribe to the surface physical adsorption of H<sub>2</sub>O [84].

Figure 7a is the EDS spectrum of NiMoO<sub>4</sub>/CoMoO<sub>4</sub> composite, which shows the surface composition of the component. The results show that the material is composed of Co, Ni, Mo, and O elements, and the ratio of Co to Ni is close to 1:1, suggesting that the sample is mainly composed of Co, Ni, Mo, and O, which is consistent with the XRD results [44, 85]. As shown in Fig. 7b–e, the element mapping images indicate the uniform distribution of Co, Ni, Mo, and O in NiMoO<sub>4</sub>/CoMoO<sub>4</sub> composite sample, suggesting the coexistence of NiMoO<sub>4</sub> and CoMoO<sub>4</sub>.

Figure 8a and b show the SEM images of synthesized NiMoO<sub>4</sub>/CoMoO<sub>4</sub> composite with Ni/Co molar ratio 1:1.

SEM images of prepared composite show grain-like morphology. The low-magnification SEM images in Fig. 8 depict the as-prepared composites are uniformly distributed on the surface of nickel foam after mild hydrothermal procedures. The aggregation of these small particles forms a porous structure, and their sizes are between 2 and 3 μm. This porous structure composite material formed on nickel foam provides abundant space and electroactive sites for electrochemical reaction, and shortens the length of diffusion path, so that its electrochemical properties can be significantly improved.

## Conclusions

In summary, NiMoO<sub>4</sub>/CoMoO<sub>4</sub> composite was successfully synthesized by an affinity hydrothermal method, which have the advantages of simplicity and cost-effectiveness. The results indicated that the as-prepared composite with the Ni/Co molar ratio of 1:1 has the best electrochemical properties, which are uniformly distributed on the surface of nickel foam with diameters between 2 and 3 μm. The specific capacitance of NiMoO<sub>4</sub>/CoMoO<sub>4</sub> composite was 2221, 1868, 1678, and 1568 F g<sup>-1</sup> at the current density of 1, 4, 7, and 10 A g<sup>-1</sup> in 3 mol L<sup>-1</sup> KOH electrolytes. In terms of specific capacitance, rate capability, cost, and simple synthesis process, its excellent electrochemical performance is satisfactory, even better than that reported in the literature, indicating its broad application prospect in high-performance SCs. The enhancement of electrochemical performance can be mainly due to the introduction of CoMoO<sub>4</sub> and the synergistic effect of cobalt molybdates and nickel molybdates, which can provide channel for quick diffusion and transport of electrons and ions and a large number of active sites.

**Funding information** This work is supported by the key R&D and Promotion Projects (Science and Technology Key Projects) of Henan Province of China (Grant Nos. 202102310226, 202102210389), and the Key Scientific Research Project of the Higher Education Institutions of Henan Province of China (Grant No. 20A530001).

## References

- Wang L, Gao H, Fang H, Wang S, Sun J (2016) Effect of methanol on the electrochemical behaviour and surface conductivity of niobium carbide-modified stainless steel for DMFC bipolar plate. *Int J Hydrog Energy* 41(33):14864–14871
- Gao H, Liao S, Zhang Y, Wang L, Zhang L (2017) Methanol tolerant core-shell RuFeSe@Pt/C catalyst for oxygen reduction reaction. *Int J Hydrog Energy* 42(32):20658–20668
- Li X, Xia T, Dong H, Shang Q, Song Y (2013) Preparation of nickel modified activated carbon/AB<sub>5</sub> alloy composite and its electrochemical hydrogen absorbing properties. *Int J Hydrog Energy* 38(21):8903–8908
- Cao Y, Zhang A-Q, Zhang H, Ding G-Q, Zhang L-S (2020) A facile route to achieve Fe<sub>2</sub>O<sub>3</sub> hollow sphere anchored on carbon nanotube for application in lithium-ion battery. *Inorg Chem Commun* 111: 107633
- Wang R, Li X, Wang Z, Zhang H (2017) Electrochemical analysis graphite/electrolyte interface in lithium-ion batteries: p-toluenesulfonyl isocyanate as electrolyte additive. *Nano Energy* 34:131–140
- Ma D, Li Y, Mi H, Luo S, Zhang P, Lin Z, Li J, Zhang H (2018) Robust SnO<sub>2-x</sub> nanoparticle-impregnated carbon nanofibers with outstanding electrochemical performance for advanced sodium-ion batteries. *Angew Chem Int Ed* 57(29):8901–8905
- Yi T-F, Zhu Y-R, Tao W, Luo S, Xie Y, Li X-F (2018) Recent advances in the research of MLi<sub>2</sub>Ti<sub>6</sub>O<sub>14</sub> (M = 2Na, Sr, Ba, Pb) anode materials for Li-ion batteries. *J Power Sources* 399:26–41
- Zhang Y, Yao Q-q, Gao H-l, Wang L-z, Jia X-l, Zhang A-q, Song Y-h, Xia T-c, Dong H-C (2014) Facile synthesis and electrochemical performance of manganese dioxide doped by activated carbon, carbon nanofiber and carbon nanotube. *Powder Technol* 262(0):150–155
- Luo S, Zhao J, Zou J, He Z, Xu C, Liu F, Huang Y, Dong L, Wang L, Zhang H (2018) Self-standing polypyrrole/black phosphorus laminated film: promising electrode for flexible supercapacitor with enhanced capacitance and cycling stability. *ACS Appl Mater* 10(4): 3538–3548
- Fang H, Meng F, Yan J, Chen G-y, Zhang L, Wu S, Zhang S, Wang L, Zhang Y (2019) Fe<sub>3</sub>O<sub>4</sub> hard templating to assemble highly wrinkled graphene sheets into hierarchical porous film for compact capacitive energy storage. *RSC Adv* 9(35):20107–20112
- Chen X, Xu G, Ren X, Li Z, Qi X, Huang K, Zhang H, Huang Z, Zhong J (2017) A black/red phosphorus hybrid as an electrode material for high-performance Li-ion batteries and supercapacitors. *J Mater Chem A* 5(14):6581–6588
- Li Y, Han X, Yi T, He Y, Li X (2019) Review and prospect of NiCo<sub>2</sub>O<sub>4</sub>-based composite materials for supercapacitor electrodes. *J Energy Chem* 31:54–78
- Li J, Wang N, Tian J, Qian W, Chu W (2018) Cross-coupled macroporous carbon network toward record high energy-power density supercapacitor at 4 V. *Adv Funct Mater* 28(51):1806153–1806161
- Chee WK, Lim HN, Zainal Z, Huang NM, Harrison I, Andou Y (2016) Flexible graphene-based supercapacitors: a review. *J Phys Chem C* 120(8):4153–4172
- Sun W, Xiao L, Wu X (2019) Facile synthesis of NiO nanocubes for photocatalysts and supercapacitor electrodes. *J Alloys Compd* 772: 465–471
- Li Q, Wei Q, Xie L, Chen C, Lu C, Su F-Y, Zhou P (2016) Layered NiO/reduced graphene oxide composites by heterogeneous assembly with enhanced performance as high-performance asymmetric supercapacitor cathode. *RSC Adv* 6(52):46548–46557
- Mohajernia S, Hejazi S, Mazare A, Nguyen NT, Hwang I, Kment S, Zoppellaro G, Tomanec O, Zboril R, Schmuki P (2017) Semimetallic core-shell TiO<sub>2</sub> nanotubes as a high conductivity scaffold and use in efficient 3D-RuO<sub>2</sub> supercapacitors. *Mater Today Energ* 6:46–52
- Zhang Y, Yao Q-q, Gao H-l, Wang L-x, Wang L-z, Zhang A-q, Song Y-h, Xia T-c (2014) Synthesis and electrochemical properties of hollow-porous MnO<sub>2</sub>-graphene micro-nano spheres for supercapacitor applications. *Powder Technol* 267(0):268–272
- Fang H, Chen G, Wang L, Yan J, Zhang L, Gao K, Zhang Y, Wang L (2018) Facile fabrication of hierarchical film composed of Co(OH)<sub>2</sub>@carbon nanotube core/sheath nanocables and its capacitive performance. *RSC Adv* 8(67):38550–38555
- Saravanakumar B, Purushothaman KK, Muralidharan G (2012) Interconnected V<sub>2</sub>O<sub>5</sub> nanoporous network for high-performance supercapacitors. *ACS Appl Mater* 4(9):4484–4490
- Li Q, Lu C, Xiao D, Zhang H, Chen C, Xie L, Liu Y, Yuan S, Kong Q, Zheng K, Yin J (2018) β-Ni(OH)<sub>2</sub> nanosheet arrays grown on biomass-derived hollow carbon microtubes for high-performance asymmetric supercapacitors. *ChemElectroChem* 5(9):1279–1287
- Fang H, Zhang LS, Xing YL, Zhang SC, Wu SD (2018) Nanostructured manganese oxide films for high performance supercapacitors. *Int J Electrochem Sci* 13(9):8736–8744
- Oudghiri-Hassani H, Al Wadaani F (2018) Preparation, characterization and catalytic activity of nickel molybdate (NiMoO<sub>4</sub>) nanoparticles. *Molecules* 23(2):273–285
- Peng S, Li L, Wu HB, Madhavi S, Lou XWD (2015) Controlled growth of NiMoO<sub>4</sub> nanosheet and nanorod arrays on various conductive substrates as advanced electrodes for asymmetric supercapacitors. *Adv Energy Mater* 5(2):1401172–1401178
- Zhang Y, Gao H-l, Jia X-d, Wang S-w, Yan J, Luo H-w, Gao K-z, Fang H, Zhang A-q, Wang L-z (2018) NiMoO<sub>4</sub> nanorods supported on nickel foam for high-performance supercapacitor electrode materials. *J Renew Sustain Ener* 10(5):054101–054110
- Fang L, Wang F, Zhai T, Qiu Y, Lan M, Huang K, Jing Q (2018) Hierarchical CoMoO<sub>4</sub> nanoneedle electrodes for advanced supercapacitors and electrocatalytic oxygen evolution. *Electrochim Acta* 259:552–558
- Li M, Yang W, Huang Y, Yu Y (2018) Hierarchical mesoporous Co<sub>3</sub>O<sub>4</sub>@ZnCo<sub>2</sub>O<sub>4</sub> hybrid nanowire arrays supported on Ni foam for high-performance asymmetric supercapacitors. *Sci China Mater* 61(9):1167–1176
- Li Q, Lu C, Chen C, Xie L, Liu Y, Li Y, Kong Q, Wang H (2017) Layered NiCo<sub>2</sub>O<sub>4</sub>/reduced graphene oxide composite as an advanced electrode for supercapacitor. *Energy Storage Mater* 8:59–67
- Lee G-H, Lee S, Kim J-C, Kim DW, Kang Y, Kim D-W (2017) MnMoO<sub>4</sub> electrocatalysts for superior long-life and high-rate lithium-oxygen batteries. *Adv Energy Mater* 7(6):1601741–1601748
- Yi T-F, Mei J, Xie Y, Luo S (2019) Hybrid porous flower-like NiO@CeO<sub>2</sub> microspheres with improved pseudocapacitive properties. *Electrochim Acta* 297:593–605
- Yi T-F, Mei J, Guan B, Cui P, Luo S, Xie Y, Liu Y (2020) Construction of spherical NiO/MnO<sub>2</sub> with core-shell structure obtained by depositing MnO<sub>2</sub> nanoparticles on NiO nanosheets for high-performance supercapacitor. *Ceram Int* 46(1):421–429
- Chen S, Yang G, Jia Y, Zheng H (2017) Three-dimensional NiCo<sub>2</sub>O<sub>4</sub>@NiWO<sub>4</sub> core-shell nanowire arrays for high performance supercapacitors. *J Mater Chem A* 5(3):1028–1034
- Nti F, Anang DA, Han JI (2018) Facilely synthesized NiMoO<sub>4</sub>/CoMoO<sub>4</sub> nanorods as electrode material for high performance supercapacitor. *J Alloys Compd* 742:342–350
- Chen S, Zhang Z, Zeng W, Chen J, Deng L (2019) Construction of NiCo<sub>2</sub>S<sub>4</sub>@NiMoO<sub>4</sub> core-shell nanosheet arrays with superior electrochemical performance for asymmetric supercapacitors. *ChemElectroChem* 6(2):590–597
- Liu M-C, Kong L-B, Lu C, Ma X-J, Li X-M, Luo Y-C, Kang L (2013) Design and synthesis of CoMoO<sub>4</sub>-NiMoO<sub>4</sub>·xH<sub>2</sub>O bundles

- with improved electrochemical properties for supercapacitors. *J Mater Chem A* 1(4):1380–1387
36. Zhu D, Shao Y (2018) NiO/ZnO nanocomposite as electrode material for supercapacitors. *Int J Electrochem Sci* 13(4):3601–3612
  37. Wang C, Guan Z, Shen Y, Yu S, Fu X-Z, Sun R, Wong C-P (2018) Shape-controlled synthesis of CoMoO<sub>4</sub>@Co<sub>1.5</sub>Ni<sub>1.5</sub>S<sub>4</sub> hybrids with rambutan-like structure for high-performance all-solid-state supercapacitors. *Chem Eng J* 346:193–202
  38. Chen C, Yan D, Luo X, Gao W, Huang G, Han Z, Zeng Y, Zhu Z (2018) Construction of core-shell NiMoO<sub>4</sub>@Ni-Co-S nanorods as advanced electrodes for high-performance asymmetric supercapacitors. *ACS Appl Mater* 10(5):4662–4671
  39. Huang Z, Zhang Z, Qi X, Ren X, Xu G, Wan P, Sun X, Zhang H (2016) Wall-like hierarchical metal oxide nanosheet arrays grown on carbon cloth for excellent supercapacitor electrodes. *Nanoscale* 8(27):13273–13279
  40. Cai D, Wang D, Liu B, Wang Y, Liu Y, Wang L, Li H, Huang H, Li Q, Wang T (2013) Comparison of the electrochemical performance of NiMoO<sub>4</sub> nanorods and hierarchical nanospheres for supercapacitor applications. *ACS Appl Mater* 5(24):12905–12910
  41. Tian X, Li X, Yang T, Wang K, Wang H, Song Y, Liu Z, Guo Q (2018) Porous worm-like NiMoO<sub>4</sub> coaxially decorated electrospun carbon nanofiber as binder-free electrodes for high performance supercapacitors and lithium-ion batteries. *Appl Surf Sci* 434:49–56
  42. Zhao Y, Teng F, Liu Z, Du Q, Xu J, Teng Y (2016) Electrochemical performances of asymmetric super capacitor fabricated by one-dimensional CoMoO<sub>4</sub> nanostructure. *Chem Phys Lett* 664:23–28
  43. Veerasubramani GK, Krishnamoorthy K, Radhakrishnan S, Kim N-J, Kim SJ (2014) Synthesis, characterization, and electrochemical properties of CoMoO<sub>4</sub> nanostructures. *Int J Hydrog Energy* 39(10):5186–5193
  44. Zhang Z, Liu Y, Huang Z, Ren L, Qi X, Wei X, Zhong J (2015) Facile hydrothermal synthesis of NiMoO<sub>4</sub>@CoMoO<sub>4</sub> hierarchical nanospheres for supercapacitor applications. *PCCP* 17(32):20795–20804
  45. Hao Y, Huang H, Wang Q, Wang Q, Zhou G (2019) Nitrogen-doped carbon/NiMoO<sub>4</sub> nanospheres assembled by nanosheets and ultrasmall nanoparticles for supercapacitors. *Chem Phys Lett* 728:215–223
  46. Sharma GP, Pala RGS, Sivakumar S (2019) Ultrasmall NiMoO<sub>4</sub> robust nanoclusters-active carbon composite for high performance extrinsic pseudocapacitor. *Electrochim Acta* 318:607–616
  47. Li J, Zhao C, Yang Y, Li C, Hollenkamp T, Burke N, Hu Z, Van Tendeloo G, Chen W (2019) Synthesis of monodispersed CoMoO<sub>4</sub> nanoclusters on the ordered mesoporous carbons for environment-friendly supercapacitors. *J Alloys Compd* 810:151841
  48. Wang J, Zhang L, Liu X, Zhang X, Tian Y, Liu X, Zhao J, Li Y (2017) Assembly of flexible CoMoO<sub>4</sub>@NiMoO<sub>4</sub>·xH<sub>2</sub>O and Fe<sub>2</sub>O<sub>3</sub> electrodes for solid-state asymmetric supercapacitors. *Sci Rep* 7:41088–41098
  49. Hu X, Zhang W, Liu X, Mei Y, Huang Y (2015) Nanostructured Mo-based electrode materials for electrochemical energy storage. *Chem Soc Rev* 44(8):2376–2404
  50. Ma X-J, Zhang W-B, Kong L-B, Luo Y-C, Kang L (2015) NiMoO<sub>4</sub>-modified MnO<sub>2</sub> hybrid nanostructures on nickel foam: electrochemical performance and supercapacitor applications. *New J Chem* 39(8):6207–6215
  51. Li Y, Jian J, Fan Y, Wang H, Yu L, Cheng G, Zhou J, Sun M (2016) Facile one-pot synthesis of a NiMoO<sub>4</sub>/reduced graphene oxide composite as a pseudocapacitor with superior performance. *RSC Adv* 6(73):69627–69633
  52. Zhang Y, Yao Q-q, Gao H-l, Zhang L-s, Wang L-z, Zhang A-q, Song Y-h, Wang L-x (2015) Synthesis and electrochemical performance of MnO<sub>2</sub>/BC composite as active materials for supercapacitors. *J Anal Appl Pyrolysis* 111:233–237
  53. Huang L, Zhang W, Xiang J, Xu H, Li G, Huang Y (2016) Hierarchical core-shell NiCo<sub>2</sub>O<sub>4</sub>@NiMoO<sub>4</sub> nanowires grown on carbon cloth as integrated electrode for high-performance supercapacitors. *Sci Rep* 6:31465–31472
  54. Zhang H, Liu J, Tian Z, Ye Y, Cai Y, Liang C, Terabe K (2016) A general strategy toward transition metal carbide/carbon core/shell nanospheres and their application for supercapacitor electrode. *Carbon* 100:590–599
  55. Zhou C, Du H, Li H, Qian W, Liu T (2019) Electrode based on nanoporous (Co-Ni)@(CoO,NiO) nanocomposites with ultrahigh capacitance after activation. *J Alloys Compd* 778:239–246
  56. Zhang L, Zheng D, Pei S, Ye L, Geng S, Lian J (2019) Rational fabrication of nanosheet-dewy NiMoO<sub>4</sub>/Ni<sub>3</sub>S<sub>2</sub> nanohybrid for efficient hybrid supercapacitor. *J Alloys Compd* 783:399–408
  57. Zhang Y, Li G-y, Lv Y, Wang L-z, Zhang A-q, Song Y-h, Huang B-l (2011) Electrochemical investigation of MnO<sub>2</sub> electrode material for supercapacitors. *Int J Hydrog Energy* 36(18):11760–11766
  58. Feng X, Ning J, Wang D, Zhang J, Xia M, Wang Y, Hao Y (2019) Heterostructure arrays of NiMoO<sub>4</sub> nanoflakes on N-doping of graphene for high-performance asymmetric supercapacitors. *J Alloys Compd* 816:152625
  59. Mei Y, Zhang H, Mei H, Kang W, Xiao Z, Zhang X, Fan W, Xu B, Hu S (2019) Effective preparation of Ni<sub>1.4</sub>Co<sub>0.6</sub>P@C micro-spheres with prolonged cycling lives for high performance hybrid supercapacitors. *J Alloys Compd* 818:152828
  60. Li B, Luo B, Zhao J, Pan Y, Zhou H, Xiao Y, Lei S, Cheng B (2019) High electrical conductivity-induced enhancement effect of electrochemical performance in mesoporous NiCo<sub>2</sub>S<sub>4</sub> nanorod-based supercapacitor. *J Energy Storage* 26:100955
  61. Chen H, Xue C, Hai Z, Cui D, Liu M, Li Y, Zhang W (2019) Facile synthesis of 3D gem shape Co<sub>3</sub>O<sub>4</sub> with mesoporous structure as electrode for high-performance supercapacitors. *J Alloys Compd* 819:152939
  62. Bhagwan J, Khaja Hussain S, Yu JS (2020) Aqueous asymmetric supercapacitors based on ZnCo<sub>2</sub>O<sub>4</sub> nanoparticles via facile combustion method. *J Alloys Compd* 815:152456
  63. Wang X, Yang Y, Zhang F, Tang J, Guo Z (2020) Facile synthesis of Co<sub>3</sub>O<sub>4</sub>/CdO nanospheres as high rate performance supercapacitors. *Mater Lett* 261:127141
  64. Faid AY, Ismail H (2019) Ternary mixed nickel cobalt iron oxide nanorods as a high-performance asymmetric supercapacitor electrode. *Mater Today Energ* 13:285–292
  65. Liu M, Shang N, Zhang X, Gao S, Wang C, Wang Z (2019) Microwave synthesis of sodium nickel-cobalt phosphates as high-performance electrode materials for supercapacitors. *J Alloys Compd* 791:929–935
  66. Huang C, Hao C, Zheng W, Zhou S, Yang L, Wang X, Jiang C, Zhu L (2019) Synthesis of polyaniline/nickel oxide/sulfonated graphene ternary composite for all-solid-state asymmetric supercapacitor. *Appl Surf Sci* Available online 5 November:144589
  67. Zhang Y, Chang C-r, Jia X-d, Huo Q-y, Gao H-l, Yan J, Zhang A-q, Ru Y, Mei H-x, Gao K-z, Wang L-z (2020) Morphology-dependent NiMoO<sub>4</sub>/carbon composites for high performance supercapacitors. *Inorg Chem Commun* 111:107631
  68. Zhu X, Hou D, Tao H, Li M (2020) Simply synthesized N-doped carbon supporting Fe<sub>3</sub>O<sub>4</sub> nanocomposite for high performance supercapacitor. *J Alloys Compd* 821:153580
  69. Liu Y, Wang Y, Chen Y, Wang C, Guo L (2020) NiCo-MOF nanosheets wrapping polypyrrole nanotubes for high-performance supercapacitors. *Appl Surf Sci* 507:145089
  70. Acharya J, Ko TH, Seo M-K, Khil M-S, Kim H-Y, Kim B-S (2020) Oxalic acid assisted rapid synthesis of mesoporous NiCo<sub>2</sub>O<sub>4</sub> nanorods as electrode materials with higher energy density and cycle stability for high-performance asymmetric hybrid supercapacitor applications. *J Colloid Interface Sci* 564:65–76

71. Zhou Y, Liu C, Li X, Sun L, Wu D, Li J, Huo P, Wang H (2019) Chemical precipitation synthesis of porous  $\text{Ni}_2\text{P}_2\text{O}_7$  nanowires for supercapacitor. *J Alloys Compd* 790:36–41
72. Wei H, Wang X, Zhang D, Du W, Sun X, Jiang F, Shi T (2019) Facile synthesis of lotus seedpod-based 3D hollow porous activated carbon/manganese dioxide composite for supercapacitor electrode. *J Electroanal Chem* 853:113561
73. Zheng Y, Tian Y, Zhang H, Guo Q, Luo J (2019) Microwave rapid synthesis of  $\text{NiO}/\text{Ni}_3\text{S}_2$ @graphite nanocomposites for supercapacitor applications. *Inorg Chem Commun* 110:107596
74. Yang Y, Ma F, Wang J, Li J, Cao J, Han W, Gu H, Zhang Y (2020) Comparative analysis of  $\text{Co}_9\text{S}_8/\text{S}$ -doped rGO composites as high-performance electrodes via facile one-step anneal fabrication for supercapacitor application. *J Alloys Compd* 815:152448
75. Zheng Y, Tian Y, Liu S, Tan X, Wang S, Guo Q, Luo J, Li Z (2019) One-step microwave synthesis of  $\text{NiO}/\text{NiS}$ @CNT nanocomposites for high-cycling-stability supercapacitors. *J Alloys Compd* 806:170–179
76. Chhetri K, Tiwari AP, Dahal B, Ojha GP, Mukhiya T, Lee M, Kim T, Chae S-H, Muthurasu A, Kim HY (2020) A ZIF-8-derived nanoporous carbon nanocomposite wrapped with  $\text{Co}_3\text{O}_4$ -polyaniline as an efficient electrode material for an asymmetric supercapacitor. *J Electroanal Chem* 856:113670
77. Zhang Y, Chang C-r, Jia X-d, Cao Y, Yan J, Luo H-w, Gao H-l, Ru Y, Mei H-x, Zhang A-q, Gao K-Z, Wang L-z (2020) Influence of metallic oxide on the morphology and enhanced supercapacitive performance of  $\text{NiMoO}_4$  electrode material. *Inorg Chem Commun* 112:107697
78. Dury F, Meixner S, Clément D, Gaigneaux EM (2005) Coupling the deoxygenation of benzoic acid with the oxidation of propylene on a Co molybdate catalyst. *J Mol Catal A Chem* 237(1):9–16
79. Yu X, Lu B, Xu Z (2014) Super long-life supercapacitors based on the construction of nanohoneycomb-like strongly coupled  $\text{CoMoO}_4$ -3D graphene hybrid electrodes. *Adv Mater* 26(7):1044–1051
80. Guo D, Zhang H, Yu X, Zhang M, Zhang P, Li Q, Wang T (2013) Facile synthesis and excellent electrochemical properties of  $\text{CoMoO}_4$  nanoplate arrays as supercapacitors. *J Mater Chem A* 1(24):7247–7254
81. Adhikary MC, Priyadarsini MH, Rath SK, Das CK (2017) 3D porous  $\text{NiMoO}_4$  nanoflakes arrays for advanced supercapacitor electrodes. *J Nanopart Res* 19(9):314–321
82. Chen S, Chandrasekaran S, Cui S, Li Z, Deng G, Deng L (2019) Self-supported  $\text{NiMoO}_4$ @ $\text{CoMoO}_4$  core/sheath nanowires on conductive substrates for all-solid-state asymmetric supercapacitors. *J Electroanal Chem* 846:113153
83. Shen J, Wang Q, Zhang K, Wang S, Li L, Dong S, Zhao S, Chen J, Sun R, Wang Y, Jian Z, Zhang W (2019) Flexible carbon cloth based solid-state supercapacitor from hierarchical holothurian-morphological  $\text{NiCo}_2\text{O}_4$ @ $\text{NiMoO}_4$ /PANI. *Electrochim Acta* 320:134578
84. Zhang H, Lu C, Hou H, Ma Y, Yuan S (2019) Tuning the electrochemical performance of  $\text{NiCo}_2\text{O}_4$ @ $\text{NiMoO}_4$  core-shell heterostructure by controlling the thickness of the  $\text{NiMoO}_4$  shell. *Chem Eng J* 370:400–408
85. Umapathy V, Neeraja P, Manikandan A, Ramu P (2017) Synthesis of  $\text{NiMoO}_4$  nanoparticles by sol-gel method and their structural, morphological, optical, magnetic and photocatalytic properties. *Trans Nonferrous Metals Soc China* 27(8):1785–1793

**Publisher's note** Springer Nature remains neutral with regard to jurisdictional claims in published maps and institutional affiliations.